ELSEVIER

Nuclear Instruments and Methods in Physics Research A 458 (2001) 518–526

NUCLEAR INSTRUMENTS & METHODS IN PHYSICS RESEARCH Section A

www.elsevier.nl/locate/nima

Experimental results from an Imarad 8×8 pixellated CZT detector

W. Li*, Z. He, G.F. Knoll, D.K. Wehe, J.E. Berry

Department of Nuclear Engineering and Radiological Sciences, University of Michigan, Ann Arbor, MI 48109, USA

Abstract

This paper reports experimental results obtained from an 8×8 pixellated CZT detector provided by Imarad Imaging Systems. Three arbitrarily selected pixels were independently tested using γ rays of different energies. The signals from an anode pixel and the cathode were read out simultaneously. From the observations of the pulse waveforms from both the anode pixel and the cathode, the electron-injection effect leading to electron–hole combination was not observed. The best energy resolution at 122 keV from the three pixels was 7.8, 6.6 and 9.4 keV, respectively, while resolution at 662 keV was 29.3, 11.8 and 26.5 keV, respectively. The electronic noise from the three pixels was similar (5 keV), so the variation in the best energy resolution indicates material nonuniformity in the detector. For the material underneath the three selected pixels, the mobility-lifetime product for electrons was measured to be 3.4, 2.4 and 1.8 ($\times 10^{-3}$ cm^2/V), respectively, and the resistivity was measured to be 8, 10 and 8.3 ($\times 10^9$ Ω cm), respectively. The variation in these results also shows the material nonuniformity across the detector. In the test with 662 keV γ rays, the pulse-height ratio of the signals from the cathode and pixel can be used to infer the interaction depth of single-pixel events. Results and analyses are presented in this paper.

Keywords: Charge transport; Pixellated CZT detector; 3-D position sensitive

1. Introduction

Room temperature pixellated semiconductor detectors are of great interest for γ-ray detection in medical, industrial and various other applications. In an effort to develop a low-cost pixellated CZT detector with high-energy resolution and large detection area, Imarad produces CZT crystals grown by the modified Bridgman method to fabricate large pixellated detectors with ohmic contacts.[1] A novel charge transport model of electron-injection and electron–hole combination was proposed in Ref. [1], and is illustrated in Fig. 1. According to this model, additional electrons are continuously injected into the detector from the cathode side while the radiation-generated electrons and holes separate due to the external electric field, and the injected electrons drift towards the holes and finally combine with them. This model differs from the conventional view of charge transport because of the role of the electron-injection mechanism. In the

* Correspondence address: PML 3061, 2301 Bonisteel Blvd., Ann Arbor, MI 48109, USA. Tel.: +1-734-7631157; fax: +1-734-7634540.

E-mail address: wenli@engin.umich.edu (W. Li).

[1] Imarad Imaging Systems LTD., Rabin Park, 10 Plaut St., Rehovot 76124, Israel.

0168-9002/01/$ - see front matter
PII: S0168-9002(00)00913-X

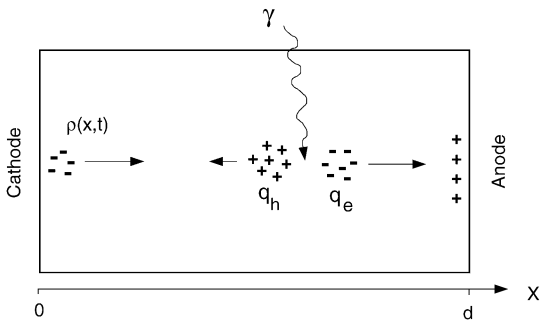

Fig. 1. Charge transport model of electron-injection and electron–hole combination.

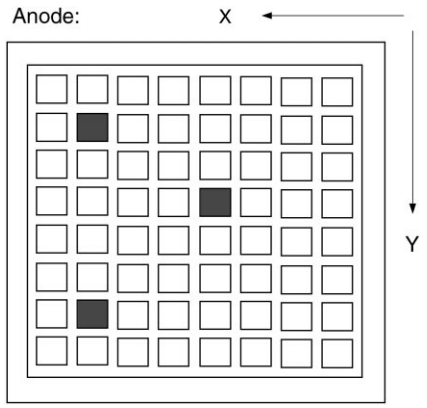

Fig. 2. Anode pattern and the locations of the three tested pixels: Pixel A (4,4), pixel B (7,2), pixel C (7,7).

conventional model, the motion of the radiation-generated charges in the detector can only cause a change in induced charge on the cathode and anode electrodes. To resolve this question of charge transport and to evaluate the performance of this kind of detector, a pixellated CZT detector provided by Imarad was tested using γ rays of different energies.

The Imarad CZT detector is a $26 \times 26 \times 4$ mm^3 crystal with an 8×8 2.5×2.5 mm^2 pixellated anode and a full single cathode. Three arbitrarily selected pixels shown in Fig. 2 were tested independently. During the tests, the signals from the cathode and the selected pixel were read out simultaneously by two Amptek preamplifiers,[2] and the eight pixels surrounding the tested pixel were grounded. The pulse waveforms and spectra from γ-radiation interactions were recorded and used diagnostically to analyze detector properties.

2. Pulse waveforms to adjudicate charge transportation models

For any pixellated CZT detector, the pulse waveforms from the cathode and anode pixel depend not only on the number and initial location of the radiation-generated charges, but also on their transport in the detector. With different charge motions, we would expect different pulse waveforms. Because the cathode signal is equally sensitive to the charge motion everywhere in the detector, the measured and expected pulse waveforms from the cathode were compared to investigate the charge transport.

In order to predict the expected pulse waveforms from the cathode, we need to find the signal currents through the cathode electrode under both charge transport models. For the electron-injection model shown in Fig. 1, consider the problem in one dimension. We need to calculate the variation of the charge density $\rho(x,t)$ to get the signal current at the cathode $i_c(t) = -\rho(0,t)v_e(v_e$ is the drift velocity of electrons). By ignoring the external detector bias we can consider the cathode and anode to have equal potential, so the integration of the electric field along any path from the cathode to the anode should be zero. According to Poisson's equation in one dimension, $\rho(x,t)$ must satisfy [3]

$$\int_0^{x_f} (d-x)\rho(x,t)\,\mathrm{d}x + q_h(d-x_h(t)) + q_e(d-x_e(t)) = 0 \quad (1)$$

where x_f is the position of the front of the injected electrons at time t. $x_e(t)$ and $x_h(t)$ are the positions of the radiation-generated electrons and holes, respectively. The $\rho(x,t)$ in Eq. (1) was solved numerically assuming electron injection for three different γ interaction depths and two different hole mobilities. The corresponding signal currents and expected preamplifier outputs from the cathode are shown in Fig. 3, together with the results from the

[2] Amptek Inc., 6 De Angelo Drive, Bedford, MA 01730, USA.

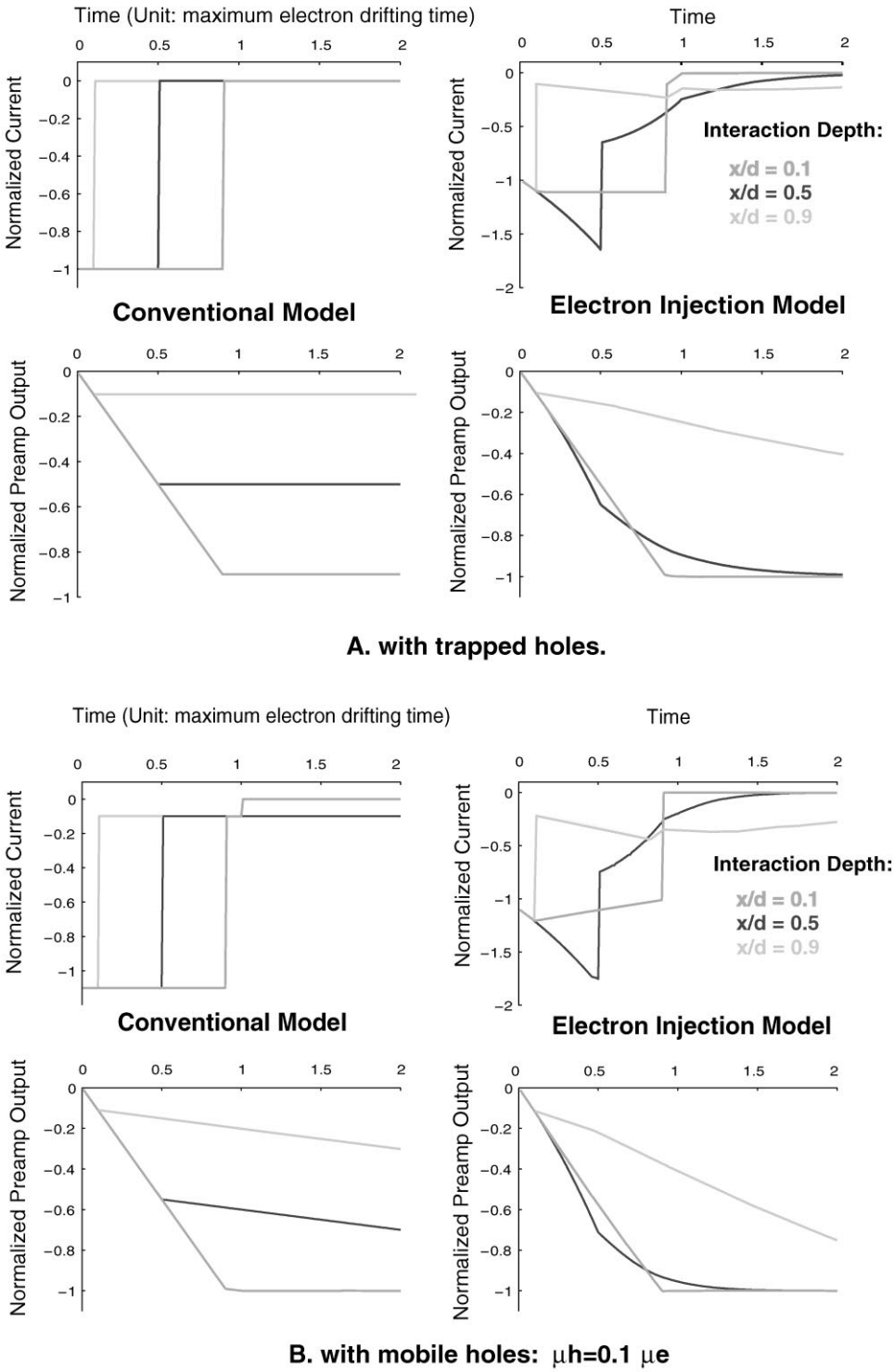

Fig. 3. Calculated signal currents and pulse waveforms for two charge transport models at three different interaction depths. (A) with trapped holes, (B) with mobile holes.

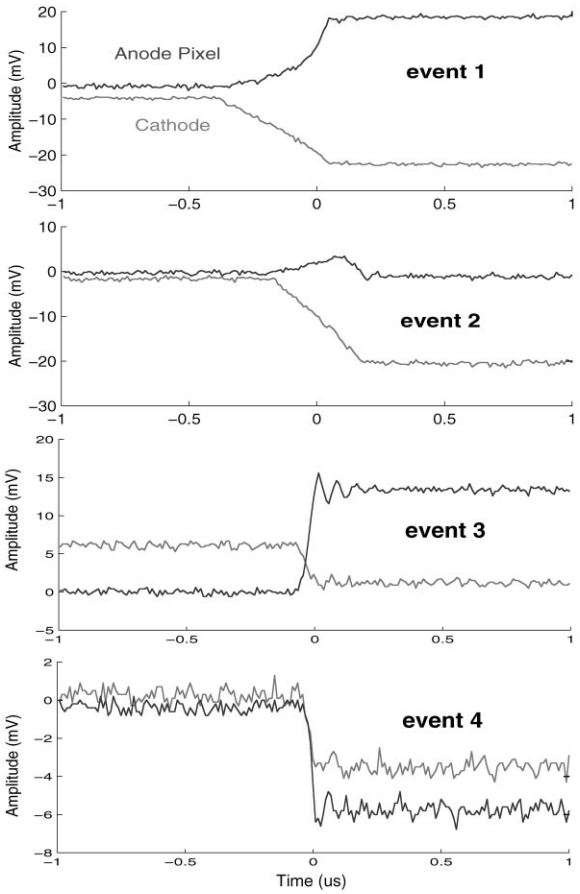

Fig. 4. Pulse waveforms from the Imarad detector.

conventional charge transport model. In the conventional model, Eq. (1) is also satisfied but with the restriction of $\rho(x,t) = \rho(t)\delta(x)$, implying no electron injection.

In the testing of the Imarad detector, the pulse waveforms from the cathode and anode pixel were recorded simultaneously. Fig. 4 shows the pulse waveforms of four typical events measured from pixel A (4,4) for Co^{60} γ rays under a -400 V cathode bias. Events 1 and 2 have similar cathode pulse waveforms with the longest rise times observed. This indicates the interaction locations of these two events were near the cathode and the electrons drifted through the entire depth of the detector. The measured cathode pulse waveforms of these two events match those expected from both charge transport models. Events 3 and 4 have cathode pulse waveforms with much shorter rise times. This means these two events occurred near the anode. These pulse waveforms match the conventional charge transport model with trapped holes, but cannot be explained by the electron-injection model. With the electron-injection model, electron injection should continue even after the collection of radiation-generated electrons, so a slow component would be expected even with fully trapped holes. But from the pulse waveforms of events 3 and 4, no such slow component was observed. It is clearly seen that after the collection of electrons there is no charge motion in the detector within the time scale of interest. This result suggests that the tested detector follows the conventional charge transport model. The pulse waveforms can also be interpreted to indicate where the electrons were collected. From Fig. 4, the electrons were collected by the tested pixel for events 1 and 3, and by an adjacent pixel for events 2 and 4.

3. Energy resolution and material properties

The uniformity of the γ-energy resolutions from different pixels of a pixellated CZT detector is usually an indication of the material uniformity across the detector [4]. For the tested Imarad detector, the energy spectra from the three tested pixels were independently collected under different detector biases using 122 keV γ rays impinging on the cathode side. The best energy resolutions from the three pixels were found using -500 V cathode bias and are shown in Fig. 5. The photopeak count rates were approximately equal. The identical readout system was used for each pixel and the electronic noise was nearly constant (monitored by the broadening of the peak from a pulser signal, as shown in Fig. 5). Nevertheless, variation in the best energy resolutions from the three tested pixels is observed. This implies different charge generation and/or trapping for the material underneath the three pixels. The energy resolution from 662 keV γ rays was also measured under varying cathode biases for each tested pixel, and the spectra with the best energy resolution are shown in Fig. 6. The significant variation in these energy resolution

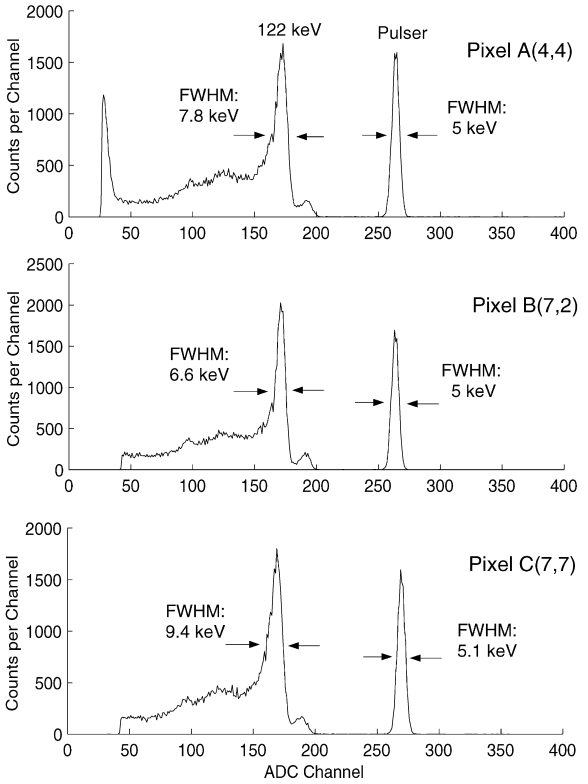

Fig. 5. 122 keV γ spectra from the three tested pixels.

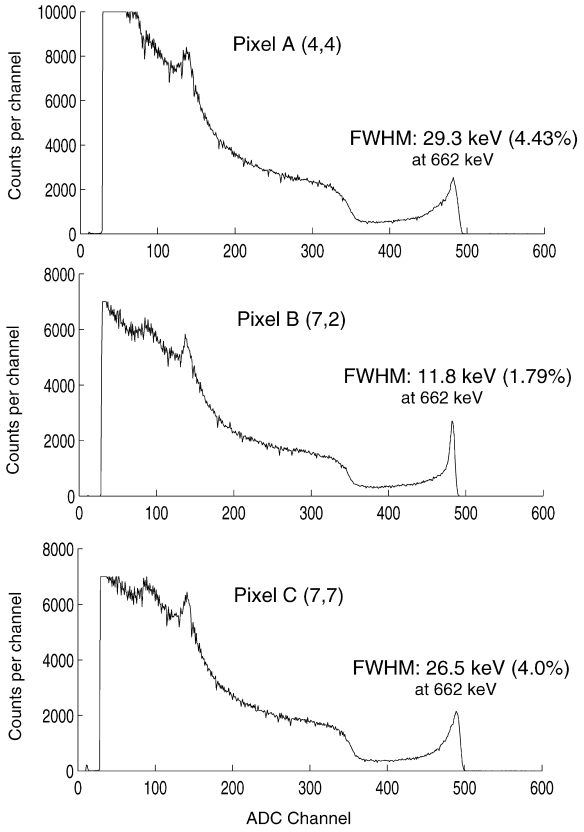

Fig. 6. 662 keV γ spectra from the three tested pixels.

also confirms the existence of some material nonuniformity under the three tested pixels.

In order to evaluate the resistivity, the leakage current through each pixel was measured under different positive and negative cathode biases. The results of the measured I–V curve as shown in Fig. 7. The linearity and symmetry of the measured I–V curves are indicative of ohmic contacts. From the slopes of the measured I–V curves the resistivities are estimated to be $8.0\times10^{9}, 1.0\times10^{10}$ and $8.3\times10^{9}\,\Omega$ cm for pixels A, B and C, respectively. While the results show good resistivity, the variation in the results indicates some material nonuniformity in the CZT crystal.

In order to evaluate the electron mobility-lifetime product of the material underneath each tested pixel, the 60 keV γ rays were used to irradiate the detector from the cathode side and the energy spectra from the cathode and tested pixel were collected under different detector biases.

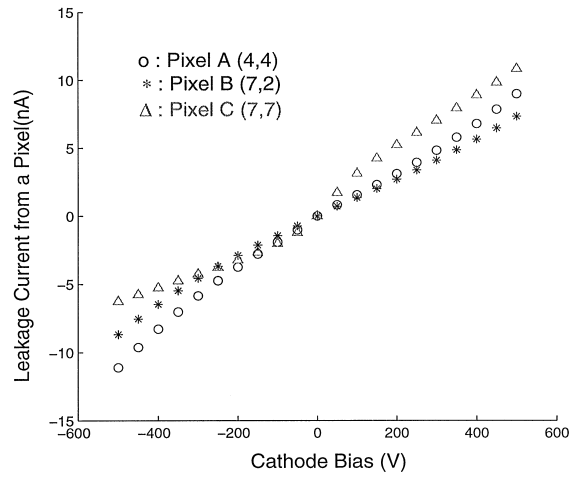

Fig. 7. I–V curves measured from the three tested pixels.

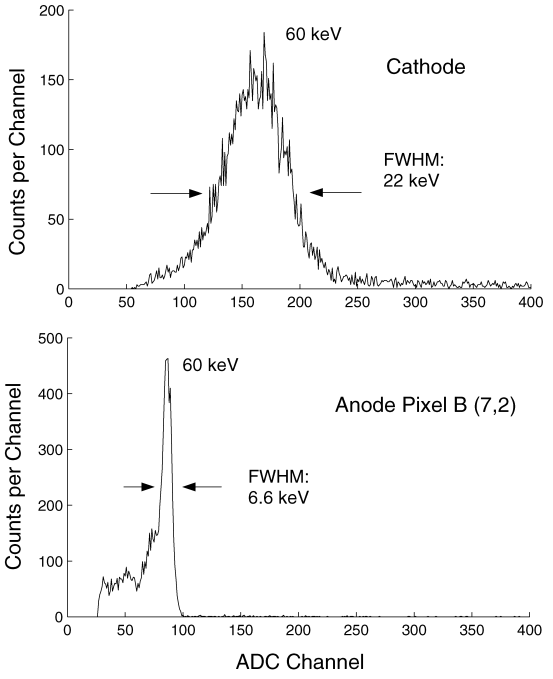

Fig. 8. 60 keV γ spectra from pixel B (7,2) and the cathode.

Fig. 8 shows the spectra collected from pixel B under -500 V cathode bias. The energy resolution from the cathode is much worse than that from the pixel because of the significantly increased electronic noise contributed from the much higher leakage current and larger detector capacitance at the cathode. When 60 keV γ rays irradiate the detector from the cathode side, most of the interactions should occur very near the cathode surface. According to Hecht relation, the photopeak centroid in the cathode spectrum is related to the detector bias V and the mobility-lifetime product of electrons $(\mu\tau)_e$:

$$\text{Centroid} = K(\mu\tau)_e V[1 - e^{-\frac{d^2}{(\mu\tau)_e V}}] \quad (2)$$

where K is a constant coefficient and d is the thickness of the detector. Fig. 9 shows the measured photopeak centroids under different detector biases. By comparing the results in Fig. 9 with Hecht curves calculated from Eq. (2) with different $(\mu\tau)_e$, the electron mobility-lifetime products can be crudely estimated as 9×10^{-4}, 9×10^{-4} and $6\times10^{-4}\,\text{cm}^2/\text{V}$ for the materials underneath pixel A, B and C, respectively.

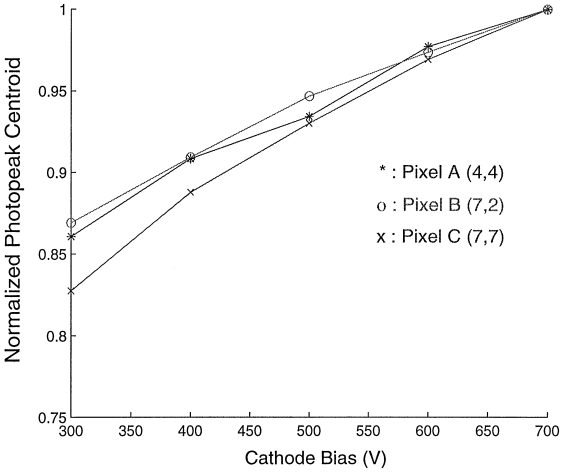

Fig. 9. Estimation of electron mobility-lifetime product from cathode spectra and Hecht relation.

As an alternative method to determine $(\mu\tau)_e$, the 60 keV photopeak centroids from an anode pixel can be used with the assumption of a perfect small pixel effect. In this case, the pulse height from the anode pixel is only determined by the number of electrons arriving at the pixel and should follow (C is a constant coefficient):

$$\text{Centroid} = Ce^{-\frac{d^2}{(\mu\tau)_e V}}. \quad (3)$$

The photopeak centroids in the spectra collected from the tested pixels under different cathode biases are shown in Fig. 10. The results are fitted to Eq. (3) and yield $(\mu\tau)_e$ of 3.4×10^{-3}, 2.4×10^{-3} and 1.8×10^{-3} cm^2/V for the material underneath pixels A, B and C, respectively. These values are larger than those from the Hecht relation method because the detector's P/D ratio (pixel-area/detector thickness) is too large to assume a perfect small pixel effect. From the pulse waveform from pixel A for event 1 in Fig. 4, we can see the motion of electrons near the cathode induce a signal on the anode pixel. The contribution from those electrons not arriving at the anode (trapped somewhere in the detector after drifting through a fraction of the detector depth) makes the signal from the pixel larger than that predicted by Eq. (3), and yields a larger estimated $(\mu\tau)_e$ than its true value. Despite the obvious systematic error, the variation in the estimated $(\mu\tau)_e$ from the different pixels indicates

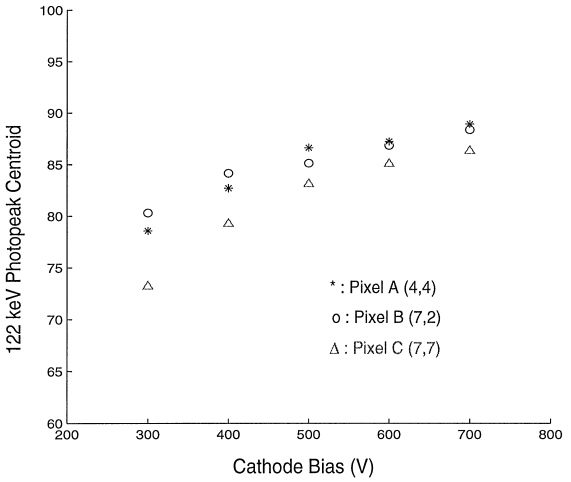

Fig. 10. Estimation of electron mobility-life time product using anode pixel spectra.

nonuniform electron trapping underneath the pixels.

4. Interaction depth sensing

Determining γ interaction depth using the C/A signal ratio has proven effective for pixellated CZT detectors with small P/D ratios (≤ 0.1) [2]. Results have not been reported for the detectors with larger P/D ratios (such as this detector with a P/D ratio of 0.63). To investigate the feasibility of interaction depth sensing for this detector, the C/A ratio was used to spatially separate the 662 keV energy spectra obtained from the anode pixel. The full range of the C/A ratios was divided into 50 equally spaced intervals, the spectrum from each interval was stored by this depth index. The minimum width of the interval depends on the uncertainty in the C/A ratio and can be derived from the fluctuations of the signals from the cathode and anode pixel. The results of the depth separation for pixel B under -600 V detector bias are shown in Figs. 11 and 12. The overall spectrum was shown in Fig. 6. In Fig. 11, spectrum A has a depth index >19, and has no 662 keV photopeak. This spectrum is from the multi-pixel events caused by electron sharing in adjacent pixels or multi-site interaction in the detector (for multi-pixel events, the signal from the tested pixel should be smaller due to charge sharing and yield larger C/A ratio). With our prime interest in depth separation for only single-pixel events, we concentrate on the spectra with depth index ≤ 19. The overall spectrum with depth index ≤ 19 is shown as spectrum B in Fig. 11 and the depth separation is shown in Fig. 12. The best energy resolution comes from the spectrum with the depth index of 16, shown as spectrum C in Fig. 11.

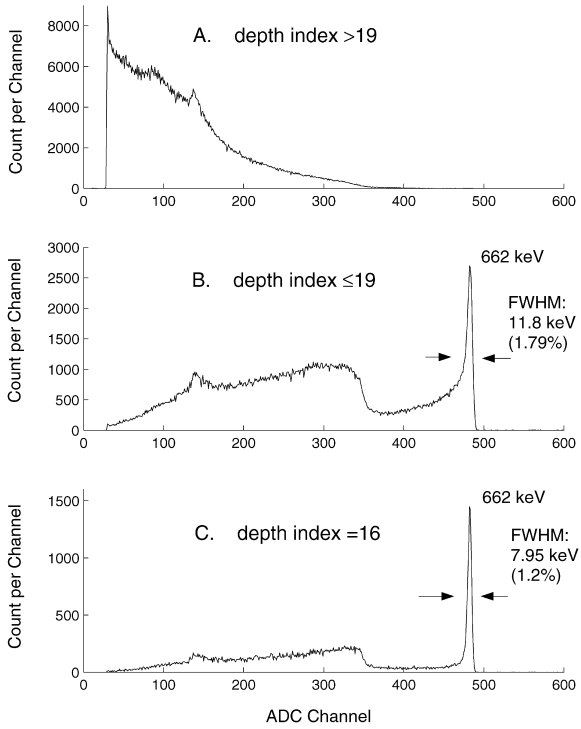

Fig. 11. 662 keV γ spectra separation from pixel B (7,2) using C/A ratio.

The photopeak centroids and areas of the spectra in Fig. 12 are calculated and shown in Fig. 13. The results are from pixel B and very similar to those from pixels A and C. The spectra for each depth index are quite consistent with earlier results and no spectrum with a double photopeak is observed. This suggests a monotonic relation between the C/A ratio and the interaction depth. Because the 662 keV γ rays interact with the detector almost uniformly along the detector depth, the distribution of photopeak area along depth index should be

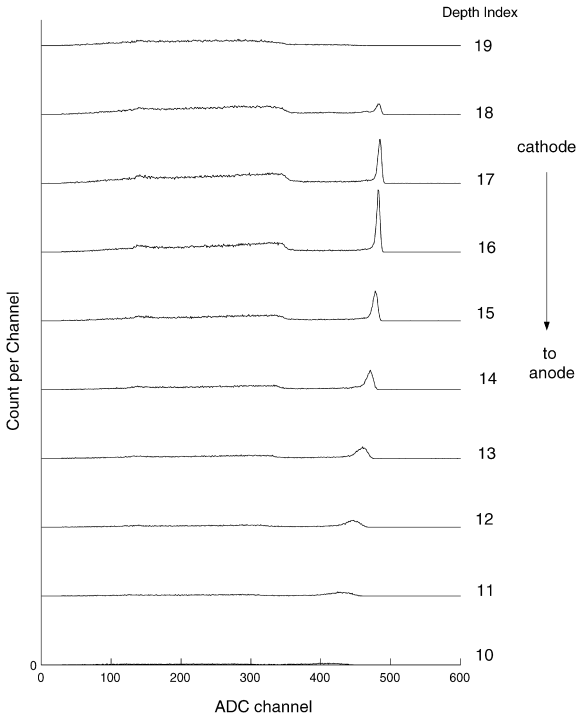

Fig. 12. Spectra from different interaction depth for pixel B (7,2).

uniform if the C/A ratio is linear to the true interaction depth. The deviation of the measured distribution from an uniform one (as shown in Fig. 13) indicates a nonlinearity in the relation between the C/A ratio and the interaction depth. The detector was modeled to check the possibility of a nonlinear but monotonic relation between the C/A ratio and the interaction depth. Assuming a uniform electric field in the detector and given mobility and mobility-lifetime products for electrons and holes, the pulse heights from the cathode and anode pixel can be calculated for the single-pixel events with given energy deposition at each interaction depth. As a result, the relationship between the C/A ratio and the interaction depth can be predicted [5]. The mobilities of electrons and holes were assumed to be 1×10^{3} and 1×10^{2} cm^2/V s, the mobility-lifetime products for electrons and holes were assumed to be 3.0×10^{-3} and 2.0×10^{-4} cm^2/V, and the weighting potential of the pixel was estimated from the published results with the same P/D ratio [6]. The result of the modeling in plot A of Fig. 14

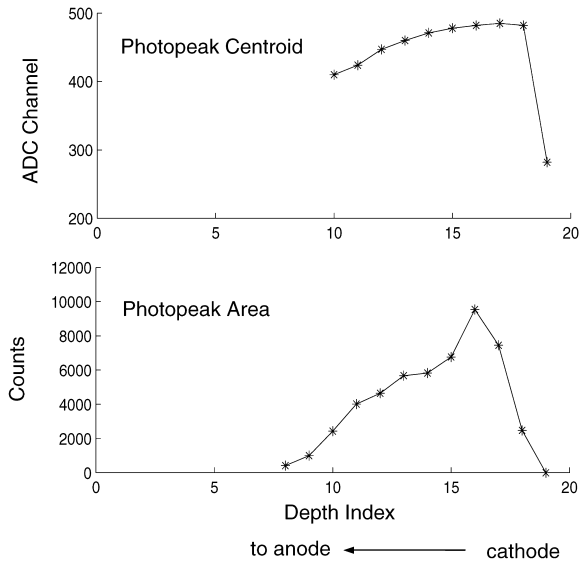

Fig. 13. Distribution of photopeak centroid and area along depth index for pixel B (7,2).

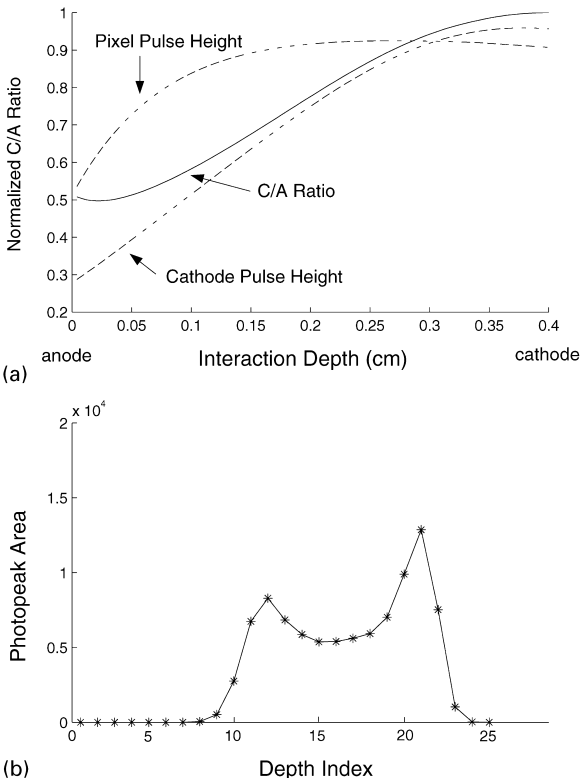

Fig. 14. Modeled results: (a) Relation between interaction depth and C/A ratio. (b) Distribution of photopeak area along depth index.

shows a nonlinear and almost monotonic relation between the C/A ratio and interaction depth. With the assumption of a uniform interaction rate at different detector depths, the distribution of photopeak area along depth index was calculated and shown in plot B of Fig. 14. This distribution is similar to that measured except for the peak that appears at the lower depth index. The events corresponding to the lower depth index are from the region near the anode, where the assumption of uniform electric field is not satisfied, which may account for this difference in the two distributions. From the overall agreement between the measured and modeled results, it seems that the C/A ratio could be used to determine the interaction depth of single-pixel events despite its large P/D ratio, particularly if a method was available to calibrate the C/A ratio to the true interaction depth.

5. Summary

A pixellated CZT detector provided by Imarad Imaging Systems has been tested to investigate charge transport models in the detector and evaluate the detector properties. Three arbitrarily selected pixels were tested independently, and the signals from each tested pixel and the cathode were read out simultaneously during the test. In the pulse waveform analysis, the measured pulse waveforms from the cathode were compared to those predicted from two different charge transport models. The results indicated that the detector follows the conventional charge transport model and no indication of electron-injection leading to electron–hole combination was observed. The resistivities and electron mobility-lifetime products were measured for the material underneath the three tested pixels. The results are consistent with good CZT detector material. Variation in these results and in the γ-energy resolutions from the three tested pixels indicates the usual material nonuniformity across the detector. The interaction depth sensing capability using the C/A ratio was investigated by comparing measurements with models of the relationship between the C/A ratio and interaction depth. The results show the C/A ratio could be used to determine the interaction depth after necessary calibration. This result may be of interest in radiation imaging applications where information about the interaction depth could be used to improve the system performance.

Acknowledgements

This work was supported under DOE Grant DOE-FG08-98NV13357.

References

[1] U. Lachish, Nucl. Instr. and Meth. A 403 (1998) 417.
[2] Z. He et al., Nucl. Instr. and Meth. A 422 (1999) 173.
[3] U. Lachish, Ohmic contact gamma radiation detectors, SPIE Conference Record, Denver, CO, 1999.
[4] W. Li et al., IEEE Trans. Nucl. Sci. NS-46 (3) (1999) 187–192.
[5] W. Li, et al., Calibration of interaction depth in 3-D position sensitive single carrier detectors, 1999 IEEE Nuclear Science Symposium, Seattle, WA, October 24–30, 1999, in preparation.
[6] J.D. Eskin et al., 1995 IEEE Nuclear Science Symposium and Medical Imaging Conference Record, Vol. 1, 1995, pp. 544–548.